Aalborg Universitet

Coordinated Primary and Secondary Frequency Support between Microgrid and Weak Grid

Xiao, Zhaoxia; Zhu, Mingke; Huang, Yu; Guerrero, Josep M.; Vasquez, Juan C.

Coordinated Primary and Secondary Frequency Support between Microgrid and Weak Grid

Xiao Zhao-xia, Zhu Mingke, Huang Yu, Josep M. Guerrero, *Fellow, IEEE*, and Juan C. Vasquez, Senior *Member, IEEE*

Abstract— **Dispersed wind power connected to the weak grid may cause the frequency instability. In this paper, a hierarchical controller applied to a microgrid (MG), including wind turbines (WT) and battery units (BU), is proposed to provide in a coordinated frequency support to a weak grid by adjusting the tie-line active power flow according to the frequency-grid requirements. The coordination between MG local and central controllers provides the following features. (i) In case of required grid-frequency, the MG tie-line power flow will be controlled to be constant in each dispatching time interval. (ii) In case of under-frequency, the coordination between WT virtual inertia and BU controllers will be used to participate in primary frequency regulation (PFR). Then, BU supplies power according to the secondary frequency regulation (SFR) commanded by the main-grid dispatch center. (iii) In case of over-frequency, BU absorbs power to reduce the tie-line active power for PFR purposes. After that, the SFR uses pitch control coordinated with the battery charge control. A stability analysis model is established to deal with several transitions among different operation modes and the interaction between the weak grid impedance and the MG output impedance. Simulation results are presented to validate the proposed approach.**

Index Terms—**Wind/battery microgrids, primary frequency regulation (PFR), secondary frequency regulation (SFR), hierarchical control, central controller, local controller**

NOMENCLATURE

Parameter	Description
W_W	Generated wind energy [J]
T	Scheduling period [min]
P_{Wf}	Forecast output power of WT [W]
P_T	Average wind power [W]
P_B^*	Reference power of the BU inverter [W]
P_{WT}	Actual WT output power [W]
P_{WT}^*	WT expected output power [W]
$P_{inertia}$	WT virtual power inertia [W]
Δf	Difference between the grid frequency and the rated one [Hz]
k	PFR factor [-]
k_d	Differential coefficient of the frequency deviation [-]
P_{AGC_MG}	AGC power scheduling of MG [W]
P_{AGC_g}	AGC power scheduling of grid[W]
C_{MG}	Frequency-regulation capacity of the MG [W]
C_g	Frequency-regulation capacity of the grid [W]
f_{min}	Minimum value of the normal frequency [Hz]
f_{max}	Maximum value of the normal frequency[Hz]
ω	WT rotor angle speed [rad/s]
ω_{rated}	WT rotor rated angle speed [rad/s]
θ	PMSG rotor position angle[°]
p	Pole pairs number of PMSG[-]
P_{sloss}	PMSG stator losses[W]
i_{sabc}	PMSG stator current[A]
U_{dc}	Back-to-back converter dc bus voltage[V]
ρ	Air density [kg/m^3]
R	WT radius[m]
C_p	Wind energy utilization factor [W·s^3/kg·m^2]
β^*	Pitch angle reference of the WT [°]
β	Pitch angle of the WT [°]
λ	Tip speed ratio[-]
C_{pmax}	maximum wind energy utilization factor [W·s^3/kg·m^2]
P_{opt}	WT maximum power [W]
L_{sd}, L_{sq}	*d-q* stator inductances [mH]
R_s	Stator resistance [Ω]
u_{sd}, u_{sq}	*d-q* stator voltages [V]
ω_e	Synchronous angular velocity[rad/s]
φ	Permanent magnet flux of the PMSG [Wb]
T_e	Electromagnetic torque of the PMSG [N·m]
E	Kinetic energy stored in the WT [J]
J	Inertia of the WT and its generator[kg·m^2]
P_f	Active power reference of the generator side converter controller [W]
P_{mpp}	MPPT output of the PMSG [W]
$P_{WTrated}$	PMSG rated power [W]
P_B^*	Active power reference of the BU inverter[W]
Q_B^*	Reactive power reference of the BU inverter[Var]
u_{gabc}	BU inverter voltages [V]
i_{Babc}	BU inverter current [A]
Z_{gdq}	Equivalent impedance of the weak grid [Ω]
P_{gref0}	Weak-grid rated power [W]
P_{gref}	Weak-grid power reference [W]
J_g	Weak-grid inertia [kg·m^2]
Z_{odq}	Equivalent output impedance of the inverter[Ω]
V_{grid}^*	Voltage magnitude of the weak grid[-]

I. INTRODUCTION

THE worldwide total installed electricity generation capacity from wind power is steadily increasing meaning that the burden

on the grid operation will increase as well [1]-[4]. Wind power fluctuations may result in grid frequency instabilities, and the situation is worse in weak-grid situations due to the small kinetic energy able to store in the generators.

In this sense, permanent magnet synchronous generators (PMSG) based wind turbines (WT) are becoming more popular in wind generation due to the higher performances required in new grid codes. In contrast to conventional synchronous generators, PMSG thanks to the use of back-to-back converters, disturbances in the wind generator little affect the main grid. However, this implies that the WT rotor speed is decoupled from the grid frequency, which may result in a lack of inertia, i.e. frequency changes may not produce power variations, as it is desired in power systems [5]-[6].

Thus, wind farms are becoming a major driver to integrate high-level penetration of renewables into the electrical grid. Nevertheless, in some large lands, like in China, due to the long distances, high voltage transmission lines are required, which can lead to an overall reduced access of wind power penetration [7]. Therefore, in order to achieve higher proportion of renewable energy access, distributed wind power generation with energy storages may be installed as well, like battery units (BU) together with wind generation to form MGs which can effectively smooth wind power fluctuations, and potentially improve the output controllability of the wind generation [8]-[9].

In case of the weak-grid conditions, the MG including WT and BU can also provide in the frequency regulation coordinated with the main grid. The main techniques to achieve wind generation participating in grid frequency regulation are virtual inertia, rotor over-speed recovery, and pitch control. These three methods are described as follows:

1) *Virtual inertia* is created to respond to frequency drops by using the kinetic energy stored in rotating masses of WTs. In case of variable speed wind turbines (VSWTs), they have more kinetic energy to be converted into electrical energy when the rotor speed of VSWTs is around the rated value [10]-[11]. Rotor inertia control can provide short-time power support along few seconds, and it may need the rotor speed recovery (RSR) control. RSR control usually requires WTs to absorb energy from the grid to restore its nominal speed. However, in [12]-[13] it was pointed out that rotor speed recovery may cause secondary frequency drop down.

2) *Rotor over-speed control* is required to regulate the rotor speed to operate over its optimal value, so that WT runs at non-maximum wind energy capture point and the rotor speed is above its optimum speed to retain part of active power standby for primary frequency regulation [14].

3) *Pitch control* aims to change the input mechanical energy of WTs by controlling the wind blade's pitch angle. Therefore, it can make the wind generation system operate below the maximum power point, giving a certain backup [15].

However, these last two methods are at the expenses of reducing the efficiency of wind generation.

A lot of work has been done in MG operation and hierarchical control has become a standard method for MG [16-19]. For an islanded MG, the control aim is to balance active power (P) and reactive power (Q) between generations and power consumption, thus making MGs to operate as a controlled voltage source. In case of grid-connected MGs including WT and EU, they usually operate as controlled current sources dependent on the capacity of the storage [20].

If the MG is connected to a weak grid, it has great responsibility on the grid frequency regulation according to the relationship between the MG and grid frequency regulation capacities. In this sense, several research works can be found about the type and size optimization of energy storages and coordination control of WT and energy storages. In [21], a flywheel is used in combination with a DFIG for grid-frequency regulation. In [22], BU is connected to the DC bus as a stationary synchronous compensator, while in [23] a super capacitor is connected to the DC bus of the PMSG wind power back-to-back converter. Although the aforementioned methods can be used to make wind generation participating in frequency regulation, a holistic control approach considering the coordination between the weak grid and MG have not been presented so far in the literature.

In order to solve the output power fluctuations and frequency instability of a WT/BU MG connected to a weak grid, this paper uses a method to calculate the expected interchanged power flow of the WT/BU MG tie-line, according to the predicted wind speed and the grid frequency inside a determined time period. When the weak grid frequency is inside a specified range, a flat tie-line power flow between MG and the grid is required. Further, when grid frequency exceeds the specified range, the output active power of the WT/BU MG is rapidly changed automatically. Then, the output power is continuously changing according to the automatic generation control (AGC) commands from the dispatch center, while the wind generation ensures maximum power point tracking (MPPT) performance. Here, a hierarchical control structure is proposed to implement a flat tie-line power flow and the primary/secondary frequency regulation (PFR and SFR) of the WT/BU MG coordinated with the weak grid. Hence, the main goals in this paper are proposed as follows :

- To design the frequency characteristic curve of BU-WT MG and develop an emulated weak grid model.
- To provide seamless coordination between a weak grid and the proposed BU-WT MG for fast frequency recovery by using automatic generation control (AGC).
- To achieve seamless coordination between BU and WT by designing a two-level control architecture for frequency participation under different operation modes.
- To develop a stability analysis model to deal with transitions among different operation modes and the interaction between the impedance of the weak grid and the output impedance of the MG.

The paper is organized as follows. Section II presents the principle of WT/BU MG to both smooth tie-line power flow and regulate grid frequency. Section III describes the WT/BU MG power and control architecture. Section IV presents the central controller including how to calculate the reference values to be sent to local controllers in different situations and operation modes. Local controllers are presented in Section V, including PMSG-side MPPT control, grid-side DC bus voltage control, virtual inertia, pitch control of WT, battery active-reactive power (PQ) control, and the emulated weak grid model with its corresponding PFR and SFR. Stability analysis is presented in Section VI. Section VII presents the simulation

results of a MG connected to the weak grid supporting frequency in different scenarios. Finally, Section VIII summarizes this paper.

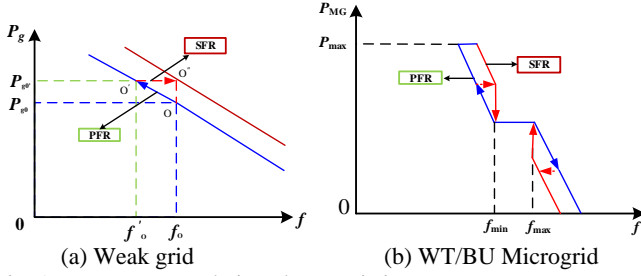## II. MICROGRID FREQUENCY SUPPORT PRINCIPLE

Fig. 1. Frequency regulation characteristics.

(a) Weak grid   (b) WT/BU Microgrid

Fig. 1 shows the static frequency regulation characteristics of (a) weak grid and (b) WT/BU MG. The weak grid will participate in the PFR and SFR by following the paralleled droop curves shown in Fig. 1(a) emulated from synchronous generators. The MG will participate in the PFR and SFR by following the hysteresis droop curves shown in Fig. 1(b) which is designed to achieve seamless coordination between weak grid and MG in grid frequency regulation. Note that both weak grid and MG has different PFR and SFR characteristics, and the aim of this work is to coordinate all of them.

Fig. 2 shows the proposed principle of the MG to regulate the grid frequency. The tie-line power flow of the MG can be controlled to be constant for a period of time when the grid frequency is within the required range, i.e. inside maximum and minimum frequencies, f_{max} and f_{min} in Fig. 1(b). If grid frequency is out of the required range, PFR and SFR will be required to provide grid-frequency restoration by changing the MG output active power in coordination with the weak-grid. Two main cases can be presented according to under/over frequency situations:

• In case that the grid-frequency is lower than required (under-frequency), virtual inertia control from the WT spinning reserve energy will be firstly used to participate in the PFR, if the rotor speed of PMSG is higher than the required value. The battery may also supply power to help the PFR, if the rotational kinetic energy is not enough. Then, if the grid frequency has not reached the required range, the battery will continue supplying

power to SFR based on the AGC reference.

• In case that the grid frequency is higher than required (over-frequency), firstly the PFR will be enabled. Thus, BU will absorb power to reduce the tie-line active power injected by the MG to the main grid, according to the difference between the actual grid frequency and the rated one. Then, the SFR will start acting so that the pitch control will be used, while the battery charge control matches the pitch control, since the response time of the pitch control is long due to the WT inertia.

III. MICROGRID POWER AND CONTROL ARCHITECTURE

Fig. 3 shows the hybrid WT/BU MG, including the power stage and the control architecture. In this case, the BU is connected to the AC side to facilitate the retrofitting of existing grid-connected wind turbines, or to easily use standard components in case of a new installation. Note that by adding batteries in the DC side may be more effective, but in practice it may not be suitable since it may require cooperation between WT and BU production companies, which may not be easy in many cases. Since in our case, the hardware control between the WT and the energy storage system is completely decoupled from each other, it is more feasible in practice.

The dispatch center is responsible for allocating the required power of the SFR to the generation units according to the load power and the generator capacity participating in the SFR of the grid, that is, the automatic generation control (AGC) command.

The central controller includes wind forecasting, tie-line power calculations, selection between operation modes, selection and reference settings of local controllers, battery charge/discharge management, and the real-time grid frequency detection. The local controllers include the virtual inertia control, MPPT algorithm and power control, DC voltage control of PMSG back-to-back converter, pitch control, and PQ control of BU inverter.

By means of the coordinated control of WT/BU, when the frequency of the system is nominal, the MG supplies flat power to the main grid. Nevertheless, when the grid frequency is outside the normal range, the MG participates with the frequency regulation, according to the principle already explained in Section II.
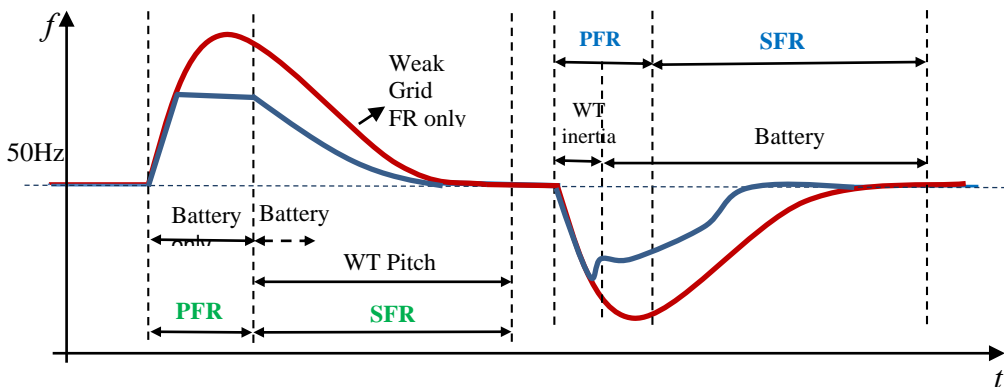

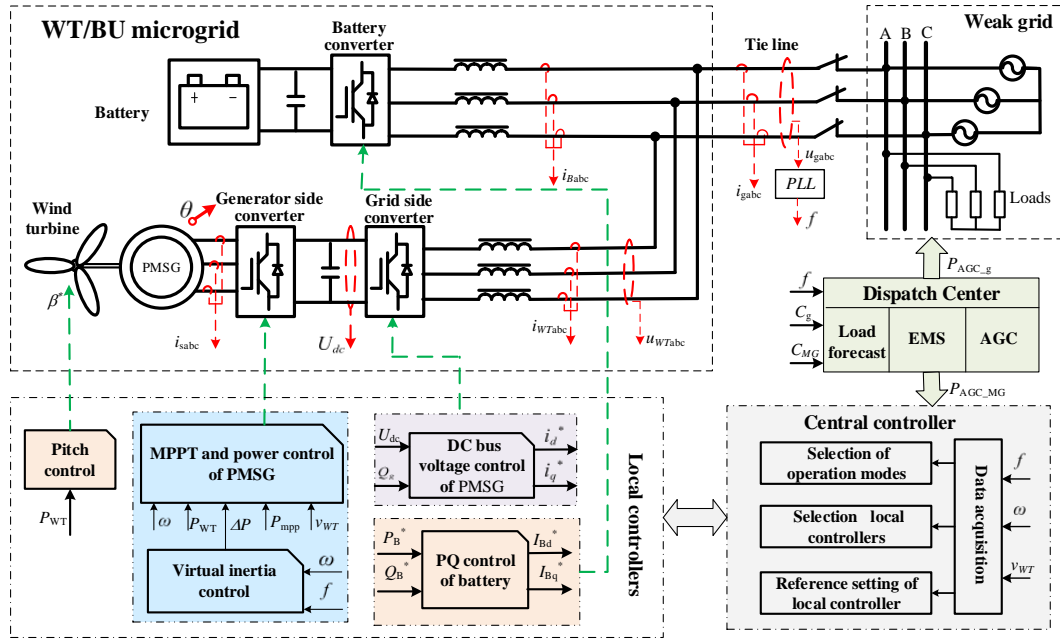Fig. 2. Proposed principle of a WT/BU MG for grid-frequency regulation.

This article has been accepted for publication in a future issue of this journal, but has not been fully edited. Content may change prior to final publication. Citation information: DOI 10.1109/TSTE.2018.2869904, IEEE Transactions on Sustainable Energy

> REPLACE THIS LINE WITH YOUR PAPER IDENTIFICATION NUMBER (DOUBLE-CLICK HERE TO EDIT) <   4

Fig. 3. Proposed WT/BU MG power and control architecture.

IV. MICROGRID CENTRAL CONTROLLER

This Section describes the different parts of the MG central controller, including reference calculations and operation modes transition conditions.

A. Local controller output power reference

1) Flat tie-line power flow

The generated wind energy W_W during the scheduling period T can be expressed as follows [22]:

$$W_w = \int_0^T P_{Wf} dt \qquad (1)$$

being P_{Wf} the forecast output power of WT derived from the forecasted wind speed. Thus, during this scheduling period T, the average wind power, P_T, can be expressed as follows:

$$P_T = W_W/T. \qquad (2)$$

If the grid frequency is nominal, the expected total output active power during the scheduling period T is the output average power. At this time, the reference power of the BU inverter can be expressed as:

$$P_B^* = P_T - P_{WT} \qquad (3)$$

where P_{WT} is the actual WT output power.

2) Primary Frequency Regulation

When the main grid requires the MG to participate in the PFR, firstly the WT will use virtual inertia control, as follows:

$$P_{inertia} = k\,\Delta f + k_d\, s\, \Delta f \qquad (4)$$

where $P_{inertia}$ is the WT virtual power inertia, the Δf is the difference between the grid frequency and the rated one, k is the PFR factor determined by the MG frequency regulation characteristics, shown in Fig. 1(b), and k_d is the differential coefficient of the frequency deviation.

Since the virtual WT inertia control will change the output power of WT automatically and the BU is responsible for smoothing the tie-line output power, the expected output active power of the BU inverter is expressed as:

$$P_B^* = P_T - P_{WT} + P_{inertia} \qquad (5)$$

If wind and rotor speeds are low, BU continues participating in the PFR, and the BU inverter power reference can be expressed as:

$$P_B^* = P_T - P_{WT} + k\,\Delta f \qquad (6)$$

where k is still the PFR factor.

Secondary Frequency Regulation

The proposed WT/BU MG is able to follow AGC power scheduling P_{AGC_MG} to restore the grid frequency for SFR purposes (see Fig. 4). The dead frequency band is defined between f_+ and f_- (±0.05Hz).
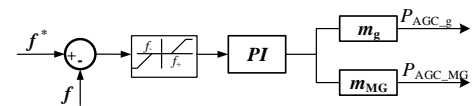
Fig. 4. Block diagram of the automatic generation control (AGC).

P_{AGC_MG} is based on the ratio between the frequency-regulation capacity of the MG and the grid from the dispatch center: $m_g = C_g/(C_g + C_{MG})$, $m_{MG} = C_{MG}/(C_g + C_{MG})$.

In case of under-frequency, the expected output active power of BU inverter is the average power plus the active power of the P_{AGC_MG}. The BU inverter reference power can be expressed as:

$$P_B^* = P_T \pm P_{AGC\_MG} - P_{WT} \qquad (7)$$

Notice that the output power of BU, P_B, should track P_B^*, which is the duty of the battery-inverter controller.

In case of over-frequency, the expected WT output active power of the pitch control can be expressed as:

$$P_{WT}^* = P_T - P_{AGC\_MG} \qquad (8)$$

where P_{WT}^* is the WT expected output power.

This article has been accepted for publication in a future issue of this journal, but has not been fully edited. Content may change prior to final publication. Citation information: DOI 10.1109/TSTE.2018.2869904, IEEE Transactions on Sustainable Energy

> REPLACE THIS LINE WITH YOUR PAPER IDENTIFICATION NUMBER (DOUBLE-CLICK HERE TO EDIT) <   5

B. Battery sizing considerations

Fig. 5. WT output power and average power.

The following considerations are needed in order to properly size the BU:

1) Minimum battery capacity proper design is necessary to flat the tie-line power flow and make it equal to the average power during T, as shown in Fig. 5. The minimum battery capacity can be obtained from the biggest area along T. Therefore, the minimum capacity of the battery can be calculated by taking half of the maximum wind energy generated during T.

2) Minimum battery charging/discharging power is designed as required to perform PFR and SFR. The maximum charging/discharging power is determined by the frequency regulation characteristics of the MG, as shown in Fig. 1(b).

C. Operation modes and transition conditions

According to Section II, there are seven operation states for both the tie-line power flat and grid frequency regulation participating purposes, as shown in Fig. 6. The functionalities of the different operation modes are described as follows.

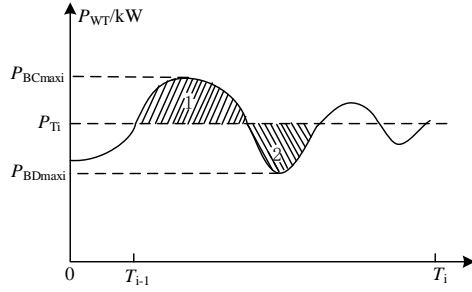- Mode 1: If $f_{min} \leq f \leq f_{max}$, the grid-frequency f will be nominal according to the grid code requirements. WT operates in MPPT mode, and tie-line active power is regulated to a constant value during this scheduling period T. Then the BU inverter active power reference is: $P_B^* = P_T - P_{WT}$.

- Mode 2: If $f < f_{min}$ and $\omega \geq 0.8\ \omega_{rated}$, virtual inertia control will be used to participate in PFR, being ω the WT rotor speed and ω_{rated} its rated value. The reference active power of WT inertia control is: $P_{inertia} = k\ f + k_d\ s\ f$. The BU inverter active power reference is: $P_B^* = P_T - P_{WT} + P_{inertia}$.

- Mode 3: If $f < f_{min}$ and $\omega < 0.7\ \omega_{rated}$, BU provides power to participate in PFR if the WT inertia is not enough. The BU inverter active power reference is: $P_B^* = P_T - P_{WT} + k \cdot \Delta f$.

- Mode 4: If $f < f_{min}$ and $\omega < 0.8\ \omega_{rated}$, WT inertia is not enough and BU provides power to participate in PFR directly and BU inverter active power reference is: $P_B^* = P_T - P_{WT} + k \cdot \Delta f$.

- Mode 5: If $f < f_{min}$, BU provides power to participate in SFR and BU inverter active power reference is: $P_B^* = P_T + P_{AGC} - P_{WT}$.

- Mode 6: If $f > f_{max}$, BU absorbs power to participate in PFR and BU inverter active power reference is: $P_B^* = P_T - P_{WT} + k \cdot \Delta f$.

- Mode 7: If $f > f_{max}$, WT pitch control is used to participate in SFR and BU absorbs power to match with the pitch control due its slow response. WT output reference active power of the pitch control is: $P_{WT}^* = P_T - P_{AGC\_MG}$. BU inverter active power reference is: $P_B^* = P_T \pm P_{AGC} - P_{WT}$.

Notice that:

i) when $\omega \geq 0.8\ \omega_{rated}$ the WT inertia is used because the kinetic energy stored in the WT is much, and when $\omega < 0.7\ \omega_{rated}$ it stops using the kinetic energy to prevent the WT shut down. In addition, the $0.7\omega_{rated}$ is chosen in order to keep a smooth speed of the WT [10, 24].

ii) when the grid frequency is too high or too low (according to the power grid standard), BU inverter power reference is greater than its charge/discharge maximum power, so that the MG may be eventually disconnected from the main grid, thus running in islanded mode.

Table I presents the transition conditions of different operation modes for the proposed WT/BU MG.

TABLE I. OPERATION MODES TRANSITION CONDITIONS

Mode	State transition condition
1	$f_{min} \leq f \leq f_{max}$
2	$(f < f_{min})\&(\omega \geq 0.8\ \omega_{rated})$
3	$(f < f_{min})\&(\omega < 0.7\ \omega_{rated})$
4	$(f < f_{min})\&(\omega < 0.8\ \omega_{rated})$
5	$(f < f_{min})\&(P_{AGC}$ command$)$
6	$f > f_{max}$
7	$(f > f_{max})\&(P_{AGC}$ command$)$

Fig. 6. Flow chart of the WT/BU MG operation modes.

V. WIND GENERATION AND BATTERY LOCAL CONTROLLERS

In this Section, the MG local controllers, including PMSG-side MPPT control, DC-bus voltage control, virtual inertia control, and WT pitch control (SubSections A-C), BU PQ control (SubSection D), and the weak grid modeling (SubSection E) are presented.

Fig. 7. Wind power MPPT control of generator-side converter.

A. MPPT control of PMSG

The WT-based PMSG use a back-to-back converter, which avoids the use of gearbox, thus improving system efficiency and reliability. The PMSG MPPT control includes outer loop based on MPPT algorithm and inner PQ control loop, as shown in Fig. 7. In this figure, θ is the rotor position angle, p is the pole pairs number, P_{sloss} is the PMSG stator losses, P_{WT} is the PMSG output active power, i_{sabc} is the PMSG stator current, and U_{dc} is the back-to-back converter dc bus voltage.

It is well known that the wind energy captured by WTs can be expressed as:

$$P_{WT} = \frac{1}{2}\rho\pi R^2 C_p v^3 \qquad (9)$$

where ρ is air density, R is the WT radius, and C_p is the wind energy utilization factor, being a function of the pitch angle β, and the tip speed ratio λ, $\lambda = \omega R/v$, while ω is the angular speed of WT. When the pitch angle is constant, the WT runs at the optimum λ, so that it can get the maximum wind energy utilization factor C_{pmax}. Therefore, the WT maximum power P_{opt} is only related to the rotor or wind speeds:

$$P_{opt} = k_1\omega^3 \qquad (10)$$
$$P_{opt} = k_2 v^3 \qquad (11)$$

where coefficients $k_1 = 0.5\rho\pi R^5 C_p \frac{\omega^3}{\lambda^3}$, and $k_2 = 0.5\rho\pi R^2 C_p$.

Usually (10) is used to calculate the maximum captured wind power since the rotor speed of PMSG is easy to be measured. When using virtual inertia control, from (11) we can calculate P_{opt} since the rotor speed will suddenly drop-down if wind kinetic energy is extracted. The transfer between these two MPPT algorithms is determined by the MG central controller.

The inner PQ control loop is designed to achieve maximum power tracking by using stator flux linkage vector control. Thus by using synchronous reference frame transformation, stator voltage equation can be expressed in dq axis:

$$\begin{cases} u_{sd} = R_S i_{sd} + L_{sd}\frac{di_{sd}}{dt} - \omega_e L_{sd} i_{sq} \\ u_{sq} = R_S i_{sq} + L_{sq}\frac{di_{sq}}{dt} + \omega_e L_{sq} i_{sd} + \omega_e\varphi \end{cases} \qquad (12)$$

The electromagnetic torque can be obtained as:

$$T_e = \frac{3}{2}p\left[\varphi i_{sq} + (L_{sd} - L_{sq})i_{sq} i_{sd}\right] \qquad (13)$$

where R_s is the stator resistance, L_{sd} and L_{sq} are the d-q stator inductances, i_{sd} and i_{sq} are the d-q stator currents, u_{sd} and u_{sq} are the d-q stator voltages, ω_e is synchronous angular velocity, and φ is permanent magnet flux linkage. Considering that d-axis current component is kept to zero, the electromagnetic torque can be expressed as:

$$T_e = \frac{3}{2}p\varphi i_{sq}. \qquad (14)$$

Therefore, we can regulate the torque or the active power by the using q-axis current component. A grid-side controller is also added to stabilize DC bus voltage of the PMSG back-to-back converter and to achieve P/Q decoupling control, similarly as in [22].

B. Virtual inertia control

Fig. 8. Rotor inertia control.

The kinetic energy stored in the WT rotor blade can be expressed as:

$$E = \frac{1}{2}J\omega^2 \qquad (15)$$

where J is the inertia of the WT and its generator, and ω is the rotor speed. When the rotor speed is ranged from ω_0 to ω_1, the WT differential kinetic energy yields to:

$$\Delta E = \frac{1}{2}J\omega_0^2 - \frac{1}{2}J\omega_1^2. \qquad (16)$$

From (16), we can conclude that WT contains certain rotational kinetic energy. Conventional VSWT, in order to achieve maximum wind energy capture, uses back-to-back converters to decouple rotor speed and grid frequency. Therefore, a frequency-dependent power command P_f can be imposed on the active power reference value of the generator side converter controller.

Fig. 8 shows the block diagram of the virtual inertia control. The virtual inertia controller can participate in PFR by linking rotor speed with frequency, taking into account speed constraints and coordinating the actions between WT and BU. When the grid frequency drops down, the controller makes the rotor speed decreasing, thus the rotating kinetic energy is released to help recovering grid frequency. When starting the virtual inertia loop, the controller will connect ΔP to switch #2 (see Fig. 8), and the power reference will change according to the frequency deviation through a PD controller that will be added over the MPPT output (P_{mpp}).

In order to prevent WT losing too much kinetic energy and self-recover its speed, when the rotor speed drop down to 0.7 times the rated value, the virtual inertia loop is disconnected and BU will support grid frequency. Hence when the system frequency is nominal, the controller will connect ΔP to switch #1, ΔP will be zero, otherwise ΔP will change according to Fig. 1(b) and the central controller. This way, stored kinetic energy

can be converted to electrical energy in order to support grid frequency.

C. Pitch control

Pitch control is used in two situations: one when wind speed exceeds the rated value and the other when grid frequency exceeds normal range. For the first situation, WT output active power needs to be limited to the rated value by changing wind turbine pitch angle β. For the second situation, WT output active power needs to be limited to the required value of the dispatch center.
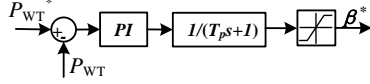

Fig.9. Block diagram of the pitch control.

Fig. 9 shows the pitch control block diagram. The WT output power P_{WT} is compared with its power reference P_{WT}^*. The error is then processed by a PI controller to produce the required β^*. Thus the pitch angle is changed accordingly, so that the WT output power is kept at reference P_{WT}^*. For instance, if $49.5 \leq f \leq 50.5$ Hz & $v > 12$m/s, $P_{WT}^* = P_{WTrated}$, where $P_{WTrated}$ is the PMSG rated power. In case of over-frequency ($f > 50.5$Hz), then $P_{WT}^* = P_T - P_{AGC\_MG}$.

D. BU Inverter P/Q Control

BU inverter power controller structure is shown in Fig. 10. Inverter voltages u_{gabc} and currents i_{Babc} are used to calculate P/Q, controlling BU output power to follow P_B^*/Q_B^*, while the inner loop limits the charging/discharging currents to the value I_{Bd}^*. The active power reference P_B^* of the BU inverter of the PFR and SFR is generated from the MG central control and the dispatch center (see Subsection IV.A). The reactive power reference Q_B^* is determined by the output power factor of the BU inverter.
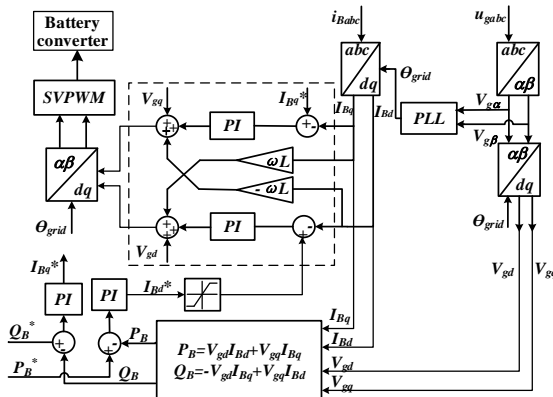
Fig. 10. Block diagram of the BU inverter power control.

The PI controller design of the MPPT control of PMSG, grid-side controller of PMSG, and the BU Inverter P/Q control is introduced in [23,24].

E. Weak-grid model

A weak grid with limited capacity is emulated by means of a controlled voltage source with a relatively large impedance Z_g, local loads, and a tie-line connected to the WT/BU MG. Fig. 11(a) shows the main circuit of the emulated weak grid, being $Z_g = R_g + jX_g$ the weak-grid impedance [25]. Note that the weak

grid has its own PFR which is governed by the swing equation, shown in Fig. 11(b), being D the droop coefficient, P_{gref0} the grid rated power, P_{gref} the grid power reference, and J_g the weak grid inertia. The SFR controllers are shown in Fig. 4 of Section IV.
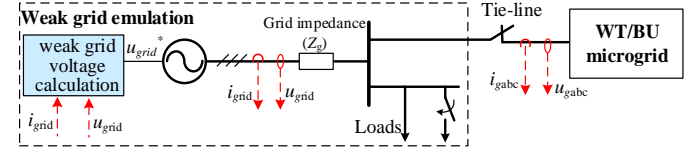
(a) Single-line main circuit of the weak grid emulation
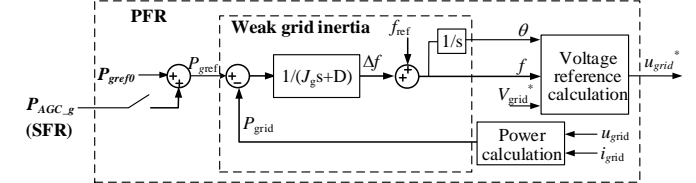
(b) Weak grid voltage calculation
Fig.11. Weak grid model.

VI. STABILITY ANALYSIS

From the operation modes of the WT-BU MG, Fig.7, Fig.10，the grid-side controller of PMSG and Fig.11 (b), the MG can be equivalent to a controlled current source with an impedance, and the weak grid can be equivalent to a controlled voltage source with an impedance as shown in Fig.12. The system stability includes two parts. The first one corresponds to the transitions among different operation modes which can be seen as a stability caused by changes in the power output from the MG to the grid. The second one is the interaction between the impedance of the weak grid and the output impedance of the MG which may also cause stability problems [26].
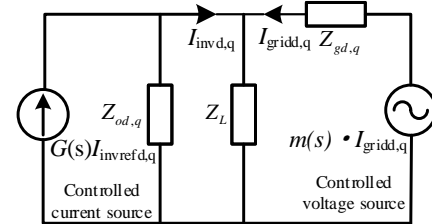

Fig.12. The equivalent system structure.

From Fig.11 (b), the math model of emulated weak grid shows as equation (17).

$$\begin{cases} f = f_{ref} + \dfrac{P_{gref} - P_{grid}}{J_g s + D} \\ \theta = \omega t = \displaystyle\int_0^t \omega dt \\ P_{grid} = u_{grid} i_{grid} \\ u_{grid}^* = V_{grid}^* \sin \theta \end{cases} \quad (17)$$

Where, V_{grid}^* is the voltage magnitude of the weak grid and constant.

The steady-state equation can be expressed in (18).

$$\begin{cases} f = f_{ref} + \dfrac{P_{gref} - P_{grid0}}{D} \\ \theta = 2\pi \displaystyle\int_0^t f dt = 2\pi ft = wt \\ P_{grid0} = V_{grid0} I_{grid0} \\ V_{grid0} = V_{grid}^* \sin \theta \end{cases} \quad (18)$$

This article has been accepted for publication in a future issue of this journal, but has not been fully edited. Content may change prior to final publication. Citation information: DOI 10.1109/TSTE.2018.2869904, IEEE Transactions on Sustainable Energy

> REPLACE THIS LINE WITH YOUR PAPER IDENTIFICATION NUMBER (DOUBLE-CLICK HERE TO EDIT) < 8

Where, V_{grid0}, I_{grid0}, P_{grid0} are the steady-state voltage, current and active power of the weak grid.

The small-signal model can be expressed in (19).

$$\begin{cases} \dfrac{d\hat{f}}{dt} = -\dfrac{D}{J_g}\hat{f} - \dfrac{1}{J_g}\hat{p}_{grid} \\ \hat{\theta} = -2\pi\dfrac{J_g}{D}\hat{f} - \dfrac{2\pi}{D}\int_0^t \hat{p}_{grid} dt \\ \hat{p}_{grid} = V_{grid0}\hat{i}_{grid} + \hat{u}_{grid}I_{grid0} \\ \hat{u}_{grid} \approx V_{grid0}\hat{\theta} \end{cases} \quad (19)$$

The frequency domain equation can be expressed as (20).

$$\begin{cases} \hat{f} = -\dfrac{V_{grid0}}{J_g s + D}(\hat{\theta}I_{grid0} + \hat{i}_{grid}) \\ \hat{\theta} = 2\pi\dfrac{J_g}{D}\dfrac{V_{grid0}}{J_g s+D}(\hat{\theta}I_{grid0}+\hat{i}_{grid}) - \dfrac{2\pi V_{grid0}}{Ds}(\hat{\theta}I_{grid0}+\hat{i}_{grid}) = \dfrac{K(s)}{1-K(s)I_{grid0}}\hat{i}_{grid} \\ \hat{u}_{grid} = V_{grid0}\dfrac{K(s)}{1-K(s)I_{grid0}}\hat{i}_{grid} = m(s)\hat{i}_{grid} \end{cases}$$

Where, $K(s) = \dfrac{2\pi J_g V_{grid0}}{DJ_g s + D^2} - \dfrac{2\pi V_{grid0}}{Ds} = -\dfrac{2\pi V_{grid0}}{J_g s^2 + Ds}$,

$m(s) = \dfrac{-2\pi V_{grid0}^2}{J_g s^2 + Ds + 2\pi P_{grid0}}$.

The grid line dq axis equation can be expressed as (21).

$$\begin{cases} \dfrac{d\hat{i}_{gd}}{dt} = \dfrac{1}{L_g}m\hat{i}_{gd} - \dfrac{1}{L_g}\hat{v}_{pccd} - \dfrac{1}{L_g}R_g\hat{i}_{gd} + \omega\hat{i}_{gq} \\ \dfrac{d\hat{i}_{gq}}{dt} = \dfrac{1}{L_g}m\hat{i}_{gq} - \dfrac{1}{L_g}\hat{v}_{pccq} - \dfrac{1}{L_g}R_g\hat{i}_{gq} - \omega\hat{i}_{gd} \end{cases} \quad (21)$$

Therefore, the equivalent impedance of the weak grid can be expressed as (22). The parameters of the weak grid will change the equivalent output impedance.

$$Z_{gdq} = -\dfrac{\hat{v}_{d,q}}{\hat{i}_{gd,q}} = sL_g + R_g - m(s) \quad (22)$$

From the Fig.10, and the grid-side controller, the inner loop current control is shown in Fig.13. The small-signal model in dq axis can be expressed as equation (23).
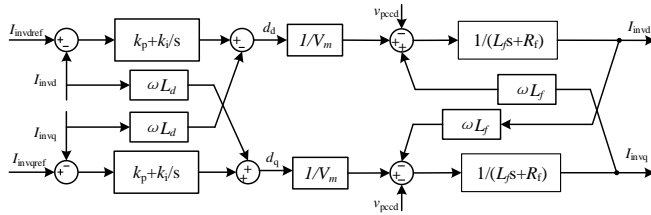

Fig.13. The d-q component block diagram when using PQ control.

$$\begin{cases} \dfrac{d\hat{i}_{invd}}{dt} = -\dfrac{1}{L_f}\hat{v}_{pccd} + \dfrac{1}{L_f}k_p(0-\hat{i}_d) + \dfrac{1}{L_f}k_i\int_0^t(0-\hat{i}_d)dt \\ \dfrac{d\hat{i}_{invq}}{dt} = -\dfrac{1}{L_f}\hat{v}_{pccq} + \dfrac{1}{L_f}k_p(0-\hat{i}_q) + \dfrac{1}{L_f}k_i\int_0^t(0-\hat{i}_q)dt \end{cases} \quad (23)$$

The transfer function can be derived as:

$$\begin{aligned} i_{iind,q} &= \dfrac{k_p s + k_i}{L_f s^2 + (k_p + R_f)s + k_i}i_{invrefd,q} - \dfrac{1}{L_f s + R_f + k_p + k_i/s}V_{pccd,q} \\ &= G(s)\cdot i_{invrefd,q} - Y(s)\cdot V_{pccd,q} \end{aligned} \quad (24)$$

From G(s), we know the system can keep stable when the reference $i_{invrefd,q}$ changes, namely the output power of the WT-BU MG changes.

The equivalent output impedance of the inverter can be expressed as (25). It is made up of a series of an inductor, a resistor and a capacitor.

$$Z_{odq} = L_f s + k_p + R_f + k_i/s \quad (25)$$

From Fig.12, in order to meet the Nyquist Criteria, the ratio Z_{gdq}/Z_{odq} should be much smaller than 1. The ratio Z_{gdq}/Z_{odq} can be expressed as.

$$N_l(s) = \dfrac{Z_{gdq}}{Z_{odq}} = \dfrac{(sL_g + R_g - m(s))//Z_l}{L_f s + k_p + R_f + k_i/s} \quad (20)$$

The frequency characteristics of Z_{gdq} and Z_{odq} are shown in Fig.14 and the Nyquist curve is shown in Fig.15 when the inductance of the grid impedance L_g changes. When the $L_g=0.6$mH, the system is not stable and has a resonance.
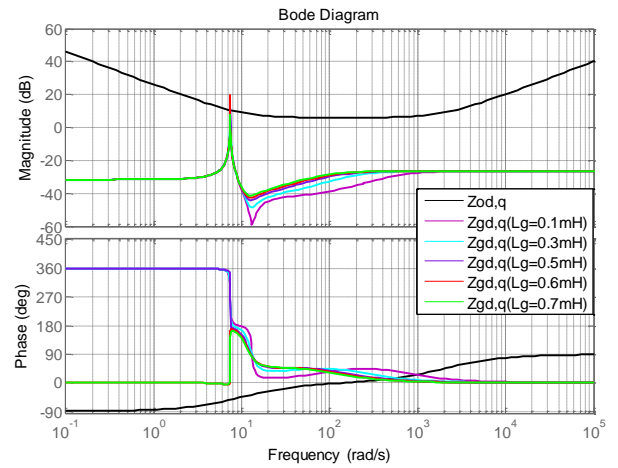

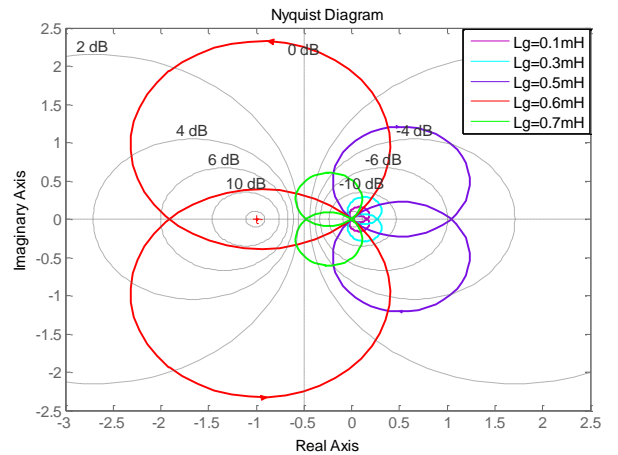Fig.14. Frequency characteristics of Z_{gdq} and Z_{odq}.

Fig.15. Nyquist diagram of the output impedance ratio when L_g changes.

VII. SIMULATION RESULTS

The model of the WT/BU MG connected through a tie-line to a weak grid was derived by using Matlab/SimPowerSystem toolbox. The selection and switching of the operating modes of the WT/BU MG embedded into the central controller are based on the *stateflow* toolbox. The main parameters of the system are

shown in Table II, including WT, PMSG, back-to-back generator-side and grid-side converter controllers, virtual inertia controller, pitch controller, battery parameters, BU-inverter controller, and the model parameters of the weak grid. The selected battery is a lithium-ion battery, which the model can be found in [27]. The rated capacity of the weak grid is 10MW, and the unit regulation power of the WT/BU MG is 500kW/Hz. The nominal grid frequency is f_n=50 Hz, with ±1% of error, so that the maximum and minimum frequencies are defined as f_{max}=50.5 Hz and f_{min}=49.5 Hz. The MG control includes flat power flow control, PFR based on the local controllers, and SFR based on AGC to restore the frequency.

TABLE II SIMULATION PARAMETERS

Wind turbine and its controller	Value
Wind turbine radius [m]	27.5
Rated wind speed [m/s]	12
Cut-in wind speed [m/s]	4
Cut-off wind speed [m/s]	20
Air density [kg/m³]	1.225
Rated power [MW]	1.1
Optimal tip speed ratio	6.325
Wind energy maximum utilization factor	0.4385
Pitch control regulator gain k_{p1}, k_{i1}, T_p	0.0012, 0.0001, 1.2
PMSG	**Value**
Rated power [MW]	1.1
Flux linkage	4.74
Inertia [kg·m2]	401258
Pole pairs	42
Rated rotor speed [rad/s]	2.7
Stator resistance [Ω]	0.006
d-axis inductance [mH]	1.704
q-axis inductance [mH]	1.216
Grid side voltage controller	**Value**
Line inductance [mH]	0.2
DC side capacitance [mF]	60
DC side rated voltage [V]	1200
Current inner loop k_{p2}, k_{i2}	1, 10
Voltage outer loop k_{p3}, k_{i3}	2, 120
Generator side controllers	**Value**
d/q axis current inner loop k_{p4}, k_{i4}	1, 10
Active power outer loop k_{p5}, k_{i5}	0.0001, 0.06
Virtual inertia control k [kW/Hz], k_d [kWs/Hz]	400, 100
BU and its controller	**Value**
Rated voltage of battery [V]	1700
Battery capacity [Ah]	100
Battery maximum charge/discharge current	3C
PQ controls d/q-axis current inner loop k_{p6}, k_{i6}	2, 20
PQ control outer loop k_{p7}, k_{i7}	0.001, 0.5
MG frequency regulation gain (f-P), k [kW/Hz]	400
Weak grid model	**Value**
Grid inertia constant J_g [kg·m2]	2.1e6
Weak grid frequency regulation gain D [kW/Hz]	500
Rated capacity P_{gref0} [MW]	10
Grid impedance Z_g [Ω]	0.1+j0.314

Wind speed curve is shown in Fig. 16, being the cut-in and cut-off wind speed fixed at 4m/s and 20m/s, and the rated wind speed at 12m/s. Meteorological real data of wind speed was provided by the Photovoltaic Research Program of Aalborg University, Denmark [23]. According to the abovementioned wind speed curve, the calculation of the tie-line active power is P_T=550kW and the reactive power Q_T=0 to make the power factor equal to 1.

Simulation results are shown in Figs. 17-25. Fig. 17 shows the grid frequency with and without the MG frequency support. The result illustrates the static frequency error reduction (from ±1Hz to ±0.5Hz which depends on the MG frequency regulation gain k). A faster frequency restoration can be seen when using MG.

Fig. 18 shows the tie-line active power when the WT/BU MG participates in the grid frequency and smooth its output power. Fig. 19 depicts the output active power of the weak grid and its reference. Notice that the difference between them is due to the PFR action at the beginning of each frequency change. Fig. 20 shows the different power of local controllers for PFR and SFR purposes. From Figs. 17 to 20, it shows the coordination of PFR and SFR between the weak grid and MG.

Fig. 21 shows the WT pitch angle dynamics. Notice that when the wind speed is lower than 12m/s, the WT operates in MPPT or SPR. While, if the wind speed is higher than 12 m/s, the pitch control will be automatically enabled.

Figs. 20 to 23, show that during under-frequency conditions, the virtual inertia helps to firstly recover the grid frequency. Then, when the stored kinetic energy is not enough, the BU restores the frequency, and the rotor speed can be self-recovered as shown in Fig.23. During over-frequency conditions, the grid frequency can be smoothly reduced due to the fast response of the BU PFR and the coordination between the pitch control and the BU SFR. Figs. 22 and 23 show WT MPPT operation (0-110s), virtual inertia operation (35-38s), and pitch control operation (110-142s and 152-162s). Fig. 24 shows that BU charge/discharge powers can accurately track P_B^*. Fig. 25 depicts the change of the BU SoC along the frequency restoration operation. Note that the SoC does not change dramatically, thus being easily recovered during normal-frequency dispatch operation periods.

The different operation states including weak grid and WT/BU MG can be observed in Table III.

TABLE III OPERATION MODES FOR WEAK GRID AND THE PROPOSED MG

Frequency(Hz)	Simulation time (s)	Weak grid	WT	BU
f=50	0-30	Maintain grid frequency and voltage	MPPT or Pitch control	Tie-line power smoothing
50>f≥49.5	30-33	PFR	MPPT	Tie-line power smoothing
f<49.5	33-36	PFR	PFR (virtual inertia)	Tie-line power smoothing
	36-49	PFR	MPPT or Pitch control	PFR and tie-line power smoothing
	49-82	SFR	MPPT or Pitch control	SFR and tie-line power smoothing
f=50	82-90	Maintain grid frequency and voltage	MPPT or Pitch control	Tie-line power smoothing
50.5≥f>50	90-93	PFR	MPPT or Pitch control	Tie-line power smoothing

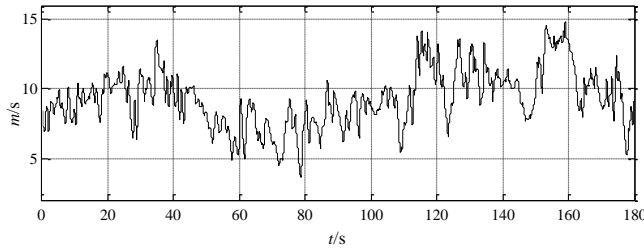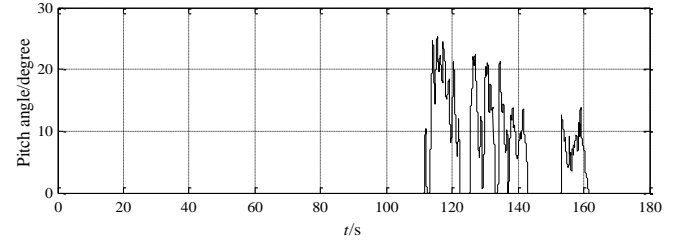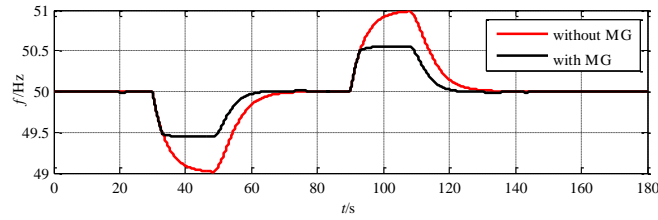|	93-108	PFR	MPPT or Pitch control	PFR and tie-line power smoothing
$f>50.5$	108-122	SFR	SFR (pitch control)	SFR and tie-line power smoothing
	122-142	SFR	SFR (pitch control)	Tie-line power smoothing
$f=50$	142-180	Maintain grid frequency and voltage	MPPT or Pitch control	Tie-line power smoothing

Fig. 16. Wind speed waveforms.

Fig.17. Grid frequency with and without MG participation.
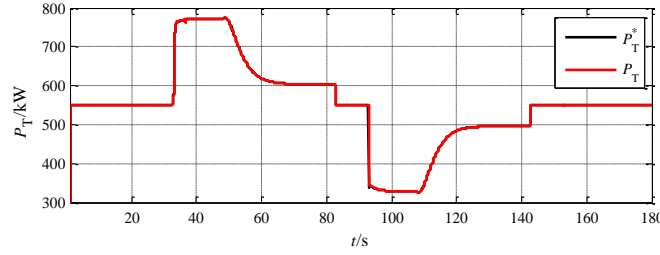
Fig. 18. The tie-line active power of WT/BU microgrid.
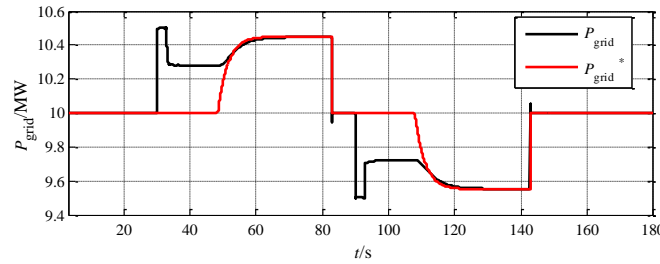
Fig. 19. The output active power of weak grid.

Fig. 20. Power reference of different PFR and SFR controllers.

Fig. 21. Pitch angle of WT.

Fig. 22. WT P_{MPPT} and P_{WT}.

Fig. 23. PMSG rotor speed.

Fig. 24. Battery charge/discharge active power (reference and actual).
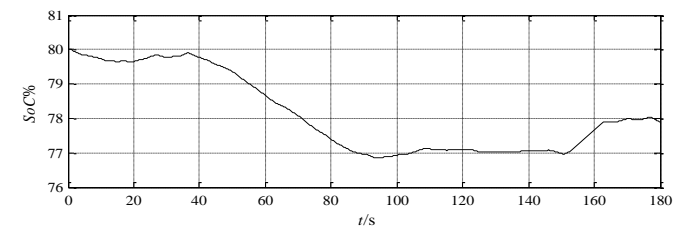

Fig. 25. Battery SoC.

VIII.   CONCLUSIONS

This paper proposed a holistic approach to regulate the frequency of a weak grid by using a WT/BU MG, with capabilities to participate in the primary and secondary frequency regulation. The proposed control architecture manages the tie-line active power of the MG according to the grid requirements, thus achieving the following functionalities:

- To provide a fast frequency recovery thanks to seamless coordination between MG and weak grid.
- To increase the whole grid inertia by the BU and virtual inertia control.
- To obtain the frequency characteristic curve of a BU-WT MG while considering weak grid model.
- To establish a stability analysis model which deals with the transitions among different operation modes and the interaction between the impedance of the weak grid and the output impedance of the MG.

As a future research work, a wind farm with energy storage participating in weak grid frequency regulation will be investigated and an advanced coordinated control will be proposed by considering different WT power ratings and energy storage capacities.

REFERENCES

[1]   J.M. Mauricio, A. Marano, A. Gómez-Expósito, J.L.M. Ramos, "Frequency regulation contribution through variable-speed wind energy conversion systems," *IEEE Trans. Power Systems*, vol. 24, no. 1, pp. 173-180, 2009.

[2]   Y. Wang, G. Delille, H. Bayem, et al., "High wind power penetration in isolated power systems—Assessment of wind inertial and primary frequency responses," *IEEE Trans. Power Systems,* vol. 28, no. 3, pp. 2412-2420, 2013.

[3]   H. J. Wang, Q. Y. Jiang , "An overview of control and configuration of energy storage system used for wind power fluctuation mitigation," *Automation of Electric Power Systems*, vol. 38, no.19, pp. 126-135, 2014.

[4]   I. D. Margaris S. A. Papathanassiou, N. D. Hatziargyriou, *et al.,* "Frequency control in autonomous power systems with high wind power penetration," *IEEE Trans. Sustainable Energy*, vol. 3, no. 2, pp. 189-199, 2012.

[5]   L. R. Chang-Chien, W. T. Lin, Y. C. Yin, "Enhancing frequency response control by DFIGs in the high wind penetrated power systems," *IEEE Trans. Power Systems*, vol. 26, no. 2, pp. 710-718, 2011.

[6]   X. Yingcheng, T. Nengling, "Review of contribution to frequency control through variable speed wind turbine," *Renewable Energy*, vol. 36, no. 6, pp. 1671-1677, 2011.

[7]   China 2050 High Proportion of Renewable Energy Development Scenarios and Paths, National Development and Reform Commission of P. R. China, 2015.

[8]   R. G. De Almeida, J.P.A. Lopes, "Participation of doubly fed induction wind generators in system frequency regulation," *IEEE Trans. Power Systems*, vol. 22, no. 3, pp. 944-950, 2007.

[9]   J. M. Mauricio, A. Marano, A. Gómez-Expósito, *et al.* "Frequency regulation contribution through variable-speed wind energy conversion systems," *IEEE Trans. Power Systems*, vol. 24, no. 1, pp. 173-180, 2009.

[10]   A. B. T. Attya, J.L. Dominguez-García, "Insights on the provision of frequency support by wind power and the impact on energy systems," *IEEE Trans. Sustainable Energy*, 2017.

[11]   G. Delille, B. Francois, and G. Malarange, "Dynamic frequency control support by energy storage to reduce the impact of wind and solar generation on isolated power system's inertia," *IEEE Trans. Sustainable Energy,* vol. 3, no. 4, pp. 931-939,2012.

[12]   G. Ramtharan, N. Jenkins, Ekanayake J B, "Frequency support from doubly fed induction generator wind turbines," *IET Renewable Power Generation,* vol. 1, no. 1, pp. 3-9, 2007.

[13]   G. Lalor, A. Mullane, M. O'Malley, "Frequency control and wind turbine technologies," *IEEE Trans. Power Systems*, vol. 20, no. 4, pp. 1905-1913, 2005.

[14]   P. K. Keung, P. Li, H. Banakar, *et al.* "Kinetic energy of wind-turbine generators for system frequency support," *IEEE Trans. Power Systems*, vol. 24, no. 1, pp. 279-287, 2009.

[15]   S. Lou, T. M. Yang, Y. W. Wu, "Coordinated optimal operation of hybrid energy storage in power system accommodated high penetration of wind power," *Automation of Electric Power Systems*, vol. 40, no.7, pp.30-35, 2016.

[16]   J. M. Guerrero, *et al.,* "Hierarchical control of droop-controlled AC and DC microgrids—A general approach toward standardization," *IEEE Trans. industrial electronics,* vol. 58, no. 1, pp. 158-172, 2011.

[17]   M. H. Amini, K. G. Boroojeni, T. Dragičević, *et al.,* "A comprehensive cloud-based real-time simulation framework for oblivious power routing in clusters of DC microgrids," DC Microgrids (ICDCM), *2017 IEEE Second International Conference on. IEEE*, pp. 270-273, 2017.

[18]   M. Kim, A. Kwasinski, "Decentralized Hierarchical Control of Active Power Distribution Nodes," *IEEE Trans. Energy Conversion,* vol. 29, no. 4, pp. 934-943, 2014.

[19]   B. Thomsen, J. M. Guerrero, P. B. Thøgersen, "Faroe islands wind-powered space heating microgrid using self-excited 220-kw induction generator," *IEEE Trans. Sustainable Energy*, vol.5, no.4, pp.1361-1366, 2014.

[20]   J. W. Choi, S. Y. Heo and M. K. Kim, "Hybrid operation strategy of wind energy storage system for power grid frequency regulation," *IET Generation, Transmission & Distribution,* vol. 10, no. 3, pp. 736-749, 2016.

[21]   P. Jiang, C. H. Xiong, "A control scheme design for smoothing wind power fluctuation with hybrid energy storage system," *Automation of Electric Power Systems*, vol. 37, no.1, pp.122-127, 2013.

[22]   N. Y. Abed, S. Teleke, and J. J. Castaneda, "Planning and operation of dynamic energy storage for improved integration of wind energy," 2011 *IEEE Power and Energy Society General Meeting*, San Diego, CA, pp. 1-7, 2011.

[23]   Z. Xiao, J. M. Guerrero, S. Jia, *et al.,* "Flat tie-line power scheduling control of grid-connected hybrid microgrids,"*Applied Energy*, vol. 210, pp. 786-799, 2018.

[24]   Xia Changliang. Operation and Control of Permanent Magnet Wind Power Generation System [M]. Science Press, 2012.

[25]   Control of a Very Weak-Grid-Connected Voltage-Source Converter Considering the Phase-Locked Loop Dynamics," *IEEE Trans. Power Electronics.* vol. 32, no. 2, pp. 977-994, 2017.

[26]   Y. Song, F. Blaabjerg, "Overview of DFIG-based wind power system resonances under weak networks," *IEEE Trans. Power Electronics*, vol. 32, no. 6, pp. 4370-4394, 2017.

[27]   T. Kim, and Q. Wei, "A hybrid battery model capable of capturing dynamic circuit characteristics and nonlinear capacity effects," *IEEE Trans. Energy Conversion*, vol. 26, no. 4, pp. 1172-1180, 2011.